https://doi.org/10.5194/egusphere-2026-6163
Preprint. Discussion started: 24 November 2026
© Author(s) 2026. CC BY 4.0 License.

A consistent and generalized actuator disk for the WRF model

Alfredo Peña[1], Oscar García-Santiago[1], Maarten Paul van der Laan[1], Branko Kosović[2], and Jeffrey D. Mirocha[3]

[1]Technical University of Denmark, DTU Wind and Energy Systems, Risø Campus, Roskilde, Denmark
[2]Johns Hopkins University, Baltimore, USA
[3]Lawrence Livermore National Laboratory, Livermore, USA

Correspondence: Alfredo Peña (aldi@dtu.dk)

Abstract. We present a modified generalized actuator disk (GAD) implementation for the Weather Research and Forecasting (WRF) model targeting large-eddy simulation domains that avoids the need for blade proprietary data. The modified implementation combines the existing procedure to account for turbine forces in the WRF model implemented by Mirocha et al. (2014) with the analytical model of body forces by Sørensen (2023). It requires commonly available turbine information only, such as thrust and power curves, rotational speed, and turbine dimensions, while retaining axial and azimuthal forcing, tip and root corrections, and wake rotation. The modified implementation also allows multiple turbine types and dimensions in the same simulation. We verify it against the original blade element momentum GAD also implemented by Mirocha et al. (2014) for a single wind turbine in a conventionally neutral boundary layer. Both GADs show similar wake structures with the modified GAD producing stronger velocity deficits and variances. The modified GAD is further demonstrated for the N4 offshore wind farm cluster, where it captures intra- and inter-farm wake effects and turbine-level power variability at affordable computational costs. The modified GAD provides a flexible and efficient alternative for high-resolution atmospheric wake simulations, particularly when detailed blade data are unavailable.

1 Introduction

The simulation of wind turbine wakes has been a central topic in the wind energy community since the late 1970s, motivated by the need to quantify power reductions and increased loading in wind farms (Lissaman, 1979). Early wake models represented turbine wakes via simplified momentum-deficit expressions aiming at evaluating wind farm layouts and energy yields (Jensen, 1983; Ainslie, 1988). Models of different fidelity, as well as methods to include turbines within flow solvers, have emerged ranging from analytical and engineering models that mostly capture the wake mean properties to Reynolds-averaged Navier–Stokes (RANS), large-eddy simulation (LES), and direct numerical simulations in which the turbine is introduced, e.g. using actuator disks (ADs) or actuator-line approaches that aim at capturing detailed wake characteristics (Vermeer et al., 2003; Troldborg, 2008; Bastankhah and Porté-Agel, 2014).

https://doi.org/10.5194/egusphere-2026-6163
Preprint. Discussion started: 24 November 2026
© Author(s) 2026. CC BY 4.0 License.

A number of numerical weather prediction (NWP) models, which are solvers of the atmospheric flow physics within the mesoscale range, also contain methods to include the impact of wind turbines on the atmosphere. Individual turbine wakes are unresolved in NWP models and their effect is parametrized as subgrid-scale sinks of momentum and, in some cases, as sources of turbulent kinetic energy (TKE). To our knowledge, the first NWP model that included turbines in the form of a wind farm parameterization (WFP), the so-called Fitch scheme (Fitch et al., 2012), was the Weather Research and Forecasting (WRF) model. Other WFPs have been implemented also in the WRF model (see e.g. Volker et al., 2015; Ma et al., 2022b; Du et al., 2025) and in other NWP models, such as MPAS (Ma et al., 2022a) and HARMONIE (van Stratum et al., 2022; Fischereit et al., 2024). WFPs in NWPs are important to study regional-scale wind farm impacts, offshore wind farm cluster wakes, and wind deployment scenarios (Hahmann et al., 2025; Dörenkämper et al., 2025). However, due to, e.g. the underlying assumptions and simplifications, and grid-scale dependence of WFPs, their ability to accurately and consistently reproduce the wake impacts is a matter of current research (Archer et al., 2020; Peña et al., 2022; García-Santiago et al., 2024).

The WRF model, among other NWP models, can be run without a parametrization for the planetary boundary layer and, if the grid spacing is sufficiently fine, is able to resolve the large scales of the turbulent flow field, while representing unresolved features with a subgrid-scale turbulence model. Such NWP models become apt for LES, which for the case of the WRF model is commonly referred to as WRF-LES. Mirocha et al. (2014) implemented a generalized actuator disk (GAD) model for WRF-LES, an implementation that represents a rotating turbine, follows the blade element momentum (BEM) theory generalization (Mikkelsen, 2003), and has a simple controller for the yaw of the turbine following the inflow direction. Following the former GAD implementation and for WRF-LES usage, an actuator line model was also implemented by Marjanovic et al. (2017). The implementation by Mirocha et al. (2014) has been used in different studies in which it has served as reference to study, e.g. the accuracy of WFPs (Peña et al., 2022), the impact of meteorological phenomena on the wake of a turbine (Arthur et al., 2020; Peña and Angelou, 2025), the impact of wakes on surface exchange (Wu et al., 2024), and wind plant blockage (Sanchez Gomez et al., 2023).

The GAD implementation by Mirocha et al. (2014) has two main practical disadvantages. First, it requires the radial distributions of aerodynamic properties of the turbine blades: the user needs to populate tabulated data for each section of the blade separately for each specific turbine. Such data are often unavailable for commercial turbines because manufacturers do not routinely disclose blade information. Second, the BEM procedure in Mirocha et al. (2014) requires an iterative solution of local induction factors for the computation of the turbine forces that can be prone to errors under complex flows. This iterative procedure can increase the computational cost, particularly when simulations are performed at high spatial resolution, over long periods, or for multiple turbines/large domains.

These limitations motivate the development of simpler AD formulations that can utilize commonly available turbine data, while retaining sufficient fidelity to accurately represent the interaction of atmospheric turbulence with the turbine wakes. Here we present a modification to the GAD implemented by Mirocha et al. (2014), which avoids the need for proprietary blade-specific aerodynamic data. This modified GAD implementation provides a computationally efficient alternative for atmospheric wake simulations, while retaining the key turbine-level effects on the atmosphere and that is compatible with momentum theory. Note that Kale et al. (2022), Bui et al. (2024), and Sanchez-Gomez et al. (2026) also developed AD implementations to

https://doi.org/10.5194/egusphere-2026-6163
Preprint. Discussion started: 24 November 2026
© Author(s) 2026. CC BY 4.0 License.

account for turbine forces for WRF-LES: the former requires proprietary blade data and the latter two do not use BEM theory and do not account for wake rotation. Our modified GAD implementation for WRF-LES is presented in Sect. 2, while Sects. 3 and 4 present the original procedure to account for the GAD forces in the WRF model, which was also implemented by Mirocha et al. (2014), and the correspondent modifications to the procedure for the modified GAD. Section 5 introduces the turbine information needed for the modified GAD implementation. Verification and demonstration of the modified GAD are performed in Sect. 6. Discussion and perspectives are presented in Sect. 7, and conclusions are presented in Sect. 8.

2 Methods

The consistent and generalized AD implementation is based on the analytical expressions of the body forces from a turbine, firstly introduced by Sørensen et al. (2020) and further improved by Sørensen (2023), combined with the procedure to introduce such forces into the momentum tendency fields developed by Mirocha et al. (2014) for WRF-LES. Section 3 details the latter procedure. In this section, we solely provide the framework related to the body forces that compose the WRF module *joukowsky_fullygeneric.F*, which is the main basis of the modified GAD. The module computes tip and hub/root corrections based on the Prandtl model (Betz, 1919) and a vortex core model, which are respectively:

$$F = (2/\pi)\arccos\left[\exp\left(-0.5N_b\sqrt{1.0+\lambda^2}(1-x_r)\right)\right] \quad \text{and} \tag{1}$$

$$G = 1-\exp\left[-a(x_r/\tilde{\delta})^b\right], \tag{2}$$

where $x_r = r/R$ is the dimensionless radial position, being r the radial distance to the considered position and R the rotor radius, N_b the number of blades, $\lambda = \Omega R/U_\infty$ the tip speed ratio, being U_∞ the free stream wind speed, Ω the rotor angular velocity, and $\tilde{\delta} = \delta/R$ a dimensionless radial distance where the maximum azimuthal velocity is achieved; here we assume $\tilde{\delta} = 0.23$, and $b = 4$ and $a = 2.335$ as in Sørensen (2023). The corrections in Eqns. (1) and (2) change with radial position and so we choose to perform computations at radial distances with a resolution of 1 m but this can easily be exchanged by, e.g. the horizontal grid spacing if sufficiently small. The main part of the procedure is the computation of the radially-integrated coefficients a_1 and a_2, which are dependent on local values of F and G in Eqns. (1) and (2):

$$a_1 = \int_0^1 \frac{G^2F^2}{x}dx, \quad \text{and} \quad a_2 = \int_0^1 GFxdx. \tag{3}$$

These two dimensionless coefficients provide an expression for the dimensionless reference circulation that represents the circulation of the optimum rotor based on a potential vortex:

$$q_0 = \left(\sqrt{(\lambda a_2)^2 + 0.5a_1C_\mathrm{T}} - \lambda a_2\right)/a_1, \tag{4}$$

where C_T is the dimensionless thrust coefficient.

https://doi.org/10.5194/egusphere-2026-6163
Preprint. Discussion started: 24 November 2026
© Author(s) 2026. CC BY 4.0 License.

We also have dimensionless thrust and power coefficients given as, respectively,

$$C_{\mathrm{T}} = \frac{T}{0.5\rho R^2 U_\infty^2} = 4\lambda \int_0^1 \frac{u_\theta}{U_\infty} x^2 dx + 2\int_0^1 \left(\frac{u_\theta}{U_\infty}\right)^2 x dx, \tag{5}$$

$$C_{\mathrm{P}} = \frac{P}{0.5\rho R^2 U_\infty^3} = 4\lambda \int_0^1 \frac{u_D}{U_\infty}\frac{u_\theta}{U_\infty} x^2 dx, \tag{6}$$

where T is the total thrust, P total power, ρ the air density, u_D the axial velocity in the rotor plane, and u_θ the azimuthal velocity in the wake just behind the rotor. The right hand side of Eqns. (5) and (6) are dimensionless forms of the result of integrating the axial and azimuthal surface forces acting on an AD, which are the two expressions that result from the combination of the equation of the pressure drop over the rotor disk and the moment of momentum equation (see Sørensen, 2023, for the details of this derivation). Notice that if we use a model for the distribution of u_θ such as

$$\frac{u_\theta}{U_\infty} = \frac{q_0}{x_r} FG, \tag{7}$$

then using Eqn. (4), Eqn. (5) can be rewritten as

$$C_{\mathrm{T}} = 4\lambda a_2 q_0 + 2a_1 q_0^2. \tag{8}$$

Similarly, by combining Eqns. (7) and (6) under the assumption of constant inflow, we can compute the ratio of the axial velocity at the rotor plane to the free streem velocity:

$$\frac{u_D}{U_\infty} = \frac{C_{\mathrm{P}}}{4\lambda a_2 q_0}. \tag{9}$$

The dimensionless forms of the axial and azimuthal surface forces can then be computed following the right hand side of Eqns. (5) and (6):

$$\tilde{f}_a = \frac{u_\theta}{U_\infty}\left(2\lambda x_r + \frac{u_\theta}{U_\infty}\right), \tag{10}$$

$$\tilde{f}_\theta = 2\left(\frac{u_D}{U_\infty}\right)\frac{u_\theta}{U_\infty}, \tag{11}$$

which, using Eqns. (7) and (9), can be rewritten as

$$\tilde{f}_a = 2q_0 GF/x_r(\lambda x_r + 0.5 q_0 GF/x_r), \tag{12}$$

$$\tilde{f}_\theta = (C_{\mathrm{P}}/2\lambda a_2) GF/x_r. \tag{13}$$

These dimensionless forces are then transformed into WRF's coordinate system, converted into machine-size dependent forces, and passed to the module *module_gen_act_disk.F* (see Sect. 3). Note that in Sørensen (2023), Eqns. (4), (7), and (9) also account for terms representing the rotation of a solid body. This term is activated when pitching the rotor to reduce the loading to maintain constant power output above wind speeds higher than rated. However, this term is turbine-type dependent, not straightforward to determine, and adds complexity to the above procedure as new radially-integrated coefficients appear but it could be introduced in a future version of the modified GAD.

https://doi.org/10.5194/egusphere-2026-6163
Preprint. Discussion started: 24 November 2026
© Author(s) 2026. CC BY 4.0 License.

3 The original generalized actuator disk procedure by Mirocha et al. (2014)

The GAD by Mirocha et al. (2014) is part of the *phys* folder, which contains the physical parametrizations and schemes within the WRF model. The main elements of the GAD are contained in */phys/module_gen_act_disk.F*, which is a module managed by */phys/module_wind_param_driver.F*, a driver coordinating the AD calls. The driver is the piece interacting with the dynamical core in the WRF model in the second part of Runge–Kutta first stage */dyn_em/module_first_rk_step_part2.F*, which applies the physics tendencies to the prognostic variables.

In the original GAD of Mirocha et al. (2014), the code in */phys/module_gen_act_disk.F* is mainly structured as follows. Note that we avoid most details that are not relevant for explaining both the idea of the original GAD procedure and the modifications to this in Sect. 4. Also note that when 'domain' is mentioned below, depending on the parallelization used, the computations are performed in patches within the domain instead of in its full extent.

1. The wind turbine information is read from a file, which is specified in the variable *windturb_spec* within the main WRF model configuration file: *namelist.input*. The *windturb_spec* file has information for each turbine of its coordinates, dimensions (hub height, rotor diameter D, blade length), turbine initial yaw position, and cut-in and cut-out wind speeds. See the details of this file and the usage of the original GAD within *namelist.input* in the *readme_original_gad.txt* in Peña (2026).

2. The horizontal positions of the inflow of each turbine within the domain are computed: the inflow is assumed to be at $1D$ upstream from the turbine location and perpendicular to the turbine plane.

3. Arrays with time series of wind speed and direction start to be populated for each turbine. Two variables (*n_timeseries* and *n_turbines*) in *namelist.input* specify the features of these time series (also detailed in *readme_original_gad.txt*). For each turbine, an instantaneous velocity normal to the rotor is computed based on the three velocity components (u, v, w) at the inflow position.

   The main loop starts for each turbine.

4. Based on a running time-average direction, the turbine rotates towards this direction at a yaw rate, if an accumulated yaw error is above a threshold. The yaw actuation is specified by the user via the variable *wp_opt* in the *namelist.input* file. An option for no yaw is also available. The turbine yaw position is thus updated.

5. Based on the running time-average velocity, a controller is set to flag the operation of the turbine within the cut-in and cut-out wind speed limits. If in operation, look-up tables (LUTs) are used to compute the rotational speed and the pitch angle of the turbine; the turbine type is specified via the variable *turbine_opt* in the *namelist.input* file. Only one turbine type per simulation is allowed and the LUTs are part of turbine-specific modules that require compilation (see e.g. *module_gad_k* in a repository with a WRF version that includes the original GAD at https://github.com/a2e-mmc/WRF, where *k* can be, e.g. nrel5 referring to the NREL 5 MW wind turbine). The assignment of the LUTs for the specific

https://doi.org/10.5194/egusphere-2026-6163
Preprint. Discussion started: 24 November 2026
© Author(s) 2026. CC BY 4.0 License.

turbine are hard-coded, so the lines with rotational speed and pitch angle computations increase if more turbine types are included. Specific turbine type is selected using the namelist variable *turbine_opt*.

6. A new loop starts to compute local lift and drag accelerations based on the instantaneous local velocities at all grid points in the domain. Tangential and normal forces are first computed based on the turbine-specific modules, which each applies the iterative BEM theory-based procedure described in the Appendix of Mirocha et al. (2014). These forces are transformed into the native x, y, z directions of the WRF model, and smeared out over the disk area before being added to the three momentum tendency fields of the WRF model. These lines also have to be hard-coded and expanded in the code if more turbine types are needed in the simulation as they come as individual turbine-specific modules. A smeared tangential force is also used to compute local turbine power that accumulates for each turbine.

4 Modifications to the original generalized actuator disk procedure

We modify the GAD procedure of Mirocha et al. (2014) in parallel to the steps outlined in Sect.3 as follows:

1. We add information of the turbine type as a last column in the *windturb_spec* file. This type value is now also used to read a turbine-specific file *wind-turbine-j.tbl*, where *j* matches the turbine type value. Further details of the turbine type and the associated files are given in Sect. 5.

2. We find the horizontal positions of the inflow of each turbine but the inflow is assumed to be at the exact turbine location.

3. For the wind speed and direction time series, we do not only compute the instantaneous velocity normal to the rotor but also the instantaneous disk-average velocity normal to the rotor at the turbine location. The amount of samples within the disk depends on the grid spacing: if not fine enough, the disk-average falls back to the value of the instantaneous velocity.

The main loop starts for each turbine.

4. The turbine yaw position is similarly updated as the original code.

5. The operation flag (same as in the original GAD) is preceded by a computation, via interpolation, of the free stream velocity U_∞ based on pre-computed LUTs of the relation U_∞-u_D, where u_D uses the running time-average disk-averaged velocity value. Since this relation is turbine specific, it is part of the information provided in the *wind-turbine-j.tbl* file. Both U_∞ and u_D are used for the operation flag: U_∞ for the cut-in/cut-out wind speed limits and u_D within its limits given by the LUTs (see Sect. 5). Values of Ω, C_T, and C_P are computed by interpolating the tables in the turbine-specific file using the current u_D on the condition that *turbine_opt=99*.

6. The loop for computation of tangential and normal forces mimics the original GAD procedure except that there is only one type of turbine option, *turbine_opt=99*, which uses the body forces framework of Sørensen (2023) for all turbine types and sizes (see Sect. 2). In the modified implementation, the forces framework is called *joukowsky_fullygeneric.F*.

https://doi.org/10.5194/egusphere-2026-6163
Preprint. Discussion started: 24 November 2026
© Author(s) 2026. CC BY 4.0 License.

Note that the instantaneous local velocities u_l are also inputs to this procedure but, in contrast to original GAD, they are converted into free stream local velocities using $1D$ momentum theory, i.e. $2u_l/\left(1+\sqrt{1-C_\mathrm{T}}\right)$, where the C_T value comes from the previous step. C_T and Ω are also inputs to *joukowsky_fullygeneric.F* as well as λ, which is computed based on the u_D-linked free stream velocity U_∞ of the previous step. A smeared tangential force is also used to compute local turbine power that accumulates for each turbine.

5 Turbine type information

One important and clear advantage of the modified GAD is the use of the turbine-specific files *wind-turbine-j.tbl*. The tabulated values in these files are pre-computed for the specific turbine: u_D, C_T, C_P, rotational speed, pitch, and U_∞. Except from u_D, the other are typical turbine performance and operation parameters generally provided by manufacturers in tabulated form. Note that we assume that in such tables, manufacturers use the free stream or ambient wind speed U_∞. Also, the module *joukowsky_fullygeneric.F* does not use currently the values in the pitch column.

We suggest to use RANS-based pre-computed values of u_D as proposed in van der Laan et al. (2015) and widely adopted in industry (see e.g. Bleeg et al., 2018). The procedure employs a single AD and calculates u_D for a range of freestream wind speeds between the turbine cut-in and cut-out wind speeds using a resolution of 1 m s^{-1}. Instead of performing a separate simulation for each inflow wind speed, we run a single RANS-AD simulation, where the inflow is kept constant, and update C_T, C_P and λ once the previous result converges following Reynolds-number similarity as detailed in van der Laan et al. (2020). This consecutive simulation of sets of C_T, C_P and λ values requires much fewer iterations compared to running a separate simulation for each wind speed. In the present work, we employ the RANS-AD method of the finite volume solver EllipSys3D (Sørensen, 1994; Mikkelsen, 2003) using the Python wind farm ecosystem PyWakeEllipSys (DTU Wind and Energy Systems, 2025).

In case, RANS-based values are not affordable, one can use $1D$ momentum theory, i.e.

$$a = 0.5\left(1-\sqrt{1-C_\mathrm{T}}\right), \quad \text{and} \quad u_D = U_\infty\,(1-a)\,, \tag{14}$$

where a is the axial induction. Such a method overpredicts U_∞ and the resulting thrust and power, as shown in van der Laan et al. (2015). Hence, we recommend using RANS-based pre-computed u_D values.

In Peña (2026), we also include two files: the turbine file *wind-turbine-99.tbl* and a Matlab (The MathWorks Inc., 2024) script *LUT_GADv2_generic_turbine.txt*. The last section of the Matlab script contains the logic that users can use and adapt to generate the turbine-specific files *wind-turbine-j.tbl*. The data in *wind-turbine-j.tbl* is linked to the WRF run via the last column of the file specified under *windturb_spec* in the *namelist.input* file; if 4 is set as the last column value, WRF expects a file *wind-turbine-4.tbl*; while if the column value is set to 99, WRF expects a file *wind-turbine-99.tbl*. To activate the modified GAD using any turbine file *wind-turbine-j.tbl*, the option *turbine_opt=99* in the *namelist.input* file is required. Note that 99 within the filename *wind-turbine-99.tbl* and the *namelist.input* file option *turbine_opt=99* are not related.

The first two sections of the Matlab script *LUT_GADv2_generic_turbine.txt* are included in case there is no information on the performance of the turbine and the user only knows its dimensions. The tabulated values in the *wind-turbine-99.tbl* file are

https://doi.org/10.5194/egusphere-2026-6163
Preprint. Discussion started: 24 November 2026
© Author(s) 2026. CC BY 4.0 License.

generated for a generic turbine, whose performance parameters are derived based on a number of turbines: the DTU 10 MW reference wind turbine (RWT), the NREL 2.8 MW RWT, the NREL 5 MW RWT, the IEA 15 MW RWT, and the IEA 22 MW RWT (Bak et al., 2013; Brown et al., 2024; Jonkman et al., 2012; Gaertner et al., 2020; Zahle et al., 2024). The procedure involves the normalization of the C_T, C_P, λ, and U_∞ values by the rated values of the five RWTs, which are then smoothly interpolated (see Fig. 1). The generic curves are hard-coded in *LUT_GADv2_generic_turbine.txt*, and since λ is turbine-size dependent, the script should be run to derive the rotational speed curve for the specific rotor diameter. If rated values are known, they can also be input into *LUT_GADv2_generic_turbine.txt*, otherwise the file also contains typical rated values. Note that we recommend to use the first two parts of the generic turbine script only in cases where there is no information available of the turbine other than its size.

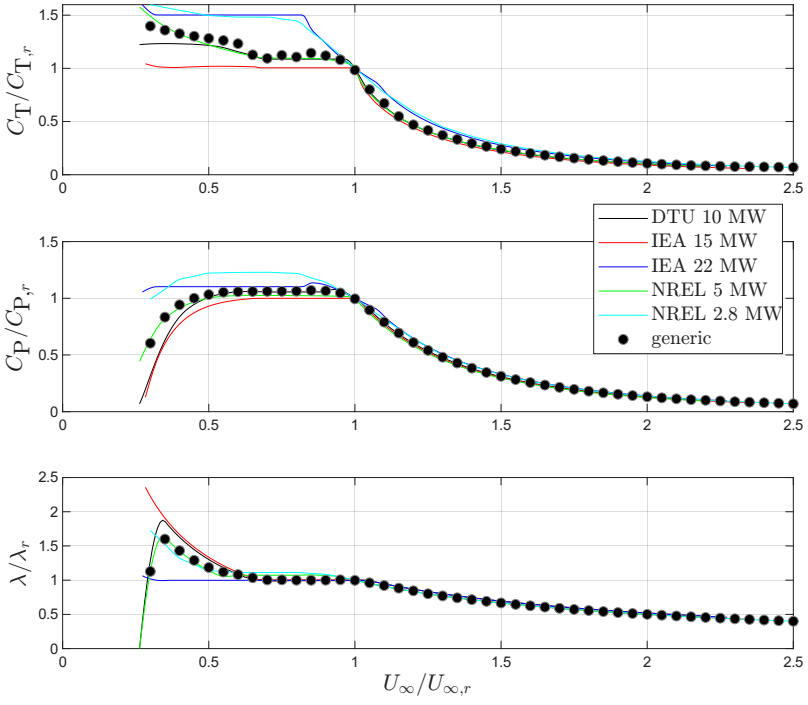

Figure 1. Generic performance curves for five research wind turbines. Normalized thrust (top) and power (middle) coefficients, and tip speed ratio (bottom) as function of the normalized free stream velocity. Subscript r denotes rated value.

6 Verification and demonstration

We verify the modified GAD implementation by performing simulations of a single wind turbine wake, in which we focus on the wake details (Sect. 6.1). Then, in Sect. 6.2 we demonstrate the modified GAD on an existing offshore wind farm cluster, in which we simulate 208 wind turbines of three different types.

https://doi.org/10.5194/egusphere-2026-6163
Preprint. Discussion started: 24 November 2026
© Author(s) 2026. CC BY 4.0 License.

6.1 Wind turbine wake

We verify the modified GAD implementation against the original BEM-based implementation by Mirocha et al. (2014), whose methods to compute the radial distribution of normal and tangential forces along the blades were previously validated against an AD implemented in RANS and blade-resolved computations from a detached eddy simulation (see details in Peña et al., 2022). Since Peña et al. (2022) used the DTU 10 MW RWT (Bak et al., 2013) for the validation of the original BEM-based procedure, for the modified GAD we choose the same turbine dimensions, i.e. hub height $z_h = 119$ m and $D = 178.33$ m. However, to show the practicalities of the generic turbine, we do not use the DTU 10 MW RWT specific C_T, C_P, λ curves but those of the generic turbine presented in Sect. 5. This means that we create a new *wind-turbine-99.tbl* file based on the generic performance curves but for the rotor diameter of the DTU 10 MW RWT using the *LUT_GADv2_generic_turbine.txt* script. The information provided in the *windturb_spec* file is identical for both original and modified GAD runs except that for the modified GAD simulations, we add a last column to the file with a value of 99 that links the turbine to the tabulated data in the file *wind-turbine-99.tbl*, which is produced using the generic curves.

6.1.1 Model setup

We configure the WRF model to run idealized simulations driven by the information from an *input_sounding* file in which the horizontal velocity components u (west-to-east) and v (north-to-south) are initialized with values of 8.28 and -0.93 m s^{-1}, respectively, at all grid points within a squared outer domain of size 15 km $\times$ 15 km with a horizontal grid spacing of 30 m. The potential temperature vertical profile is the same for all grid points within that domain, except that the temperature is constant and dry (289 K) up to a height of 700 m and increases 1 K every 1000 m upwards. We therefore aim at modeling a conventionally neutral boundary layer as inflow. Within the outer domain, we one-way nest a smaller domain of 5 km $\times$ 5 km with a horizontal spacing of 10 m.

Both domains have 120 grid points in the vertical direction with a vertical spacing of ≈5 m within the first 250 m. This spacing is increased up to a height of ≈900 m, reaching a vertical spacing of 35 m, which is maintained up to the model top at 2000 m. The outer domain is periodic in all lateral boundaries to allow the development of the atmospheric turbulent boundary layer. Both domains are run in LES mode and use the subgrid-scale model of Deardorff (1980). The bottom of both domains is flat with a roughness length of 0.0002 m. Surface conditions are connected to the atmosphere via a similarity-theory-based surface-layer scheme in the WRF model with a surface heat flux of zero. The latitude was set to 54.45°.

After a spin up of 10 hr, we perform three restart runs, one without and two including the turbine in the middle of the inner domain, i.e. $(x_o, y_o) = (2500, 2500)$ m, for one more hour. The two including the turbine are run with the original and the modified GAD, respectively, and statistics of the LES fields are computed for the last 30 min. The two-domain configuration and the turbine in the inner domain are shown in Fig. 2, which also portraits an instantaneous horizontal plane of the u-velocity component at 119 m after one hour of simulation with the turbine using the modified GAD. The initial velocity values in the *input_sounding* file are chosen so that after spin up time, the flow at hub height is nearly parallel to the grid (west-east) with an average horizontal velocity of ≈ 8 m s^{-1} at hub height, which is typically below rated speed.

https://doi.org/10.5194/egusphere-2026-6163
Preprint. Discussion started: 24 November 2026
© Author(s) 2026. CC BY 4.0 License.

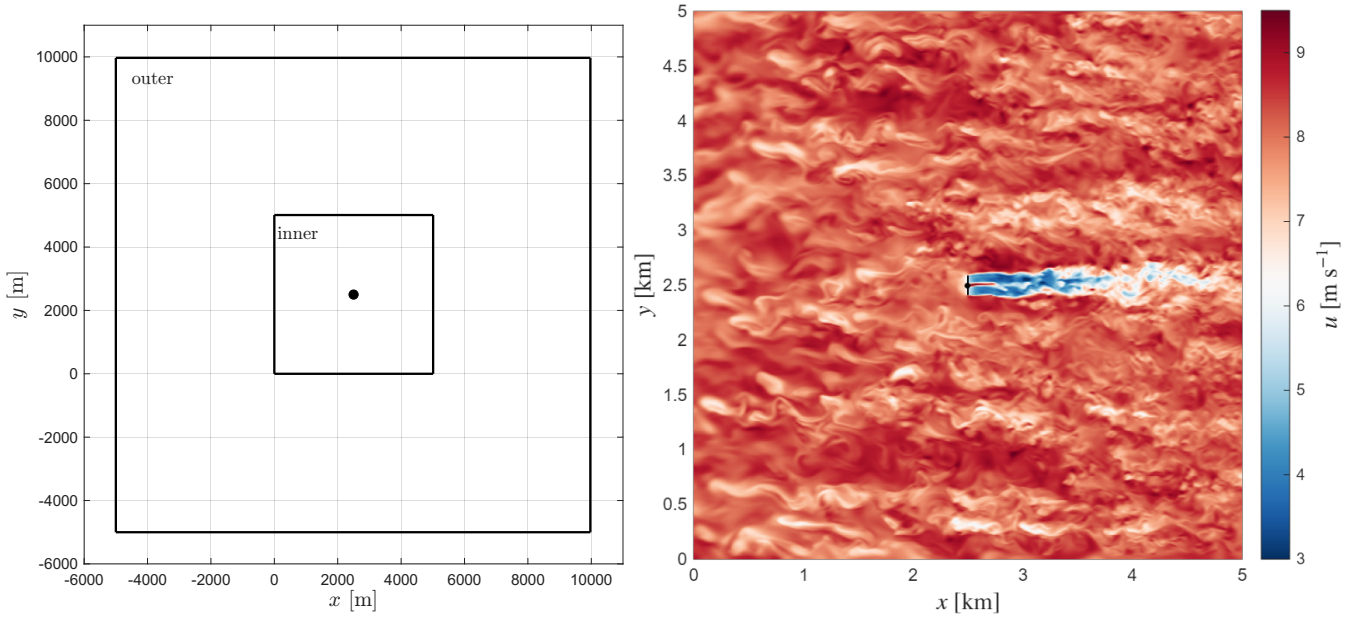

Figure 2. (left) The two-domains configuration of the single wind turbine wake. (right) Horizontal plane of the instantaneous u-velocity component at 119 m after introducing the turbine for 30 min in the inner most domain using the modified GAD.

6.1.2 Results

For the single wind turbine case, we output horizontal slices every 10 s of the three velocity components at 23 vertical levels starting at a height of 19 m up to 239 m every 10 m. Based on these slices, vertical planes at the first grid point east of the position of the turbine are extracted and time-averaged for the three velocity components for both the original and modified GAD runs. These planes are shown in Figure 3.

On purpose, we do not smooth the contour plots in Fig. 3 and keep the limits in the colorbar of the specific run and velocity to clearly visualize the details of each GAD approach. Both the original and modified GAD qualitatively show similar results: a u-velocity field mainly driven by the turbine thrust, and v- and w-velocities portraying the divergence of the flow by the rotating GAD. However, we already notice a stronger wake deficit, i.e. stronger reduction of the axial velocity, leading to lower values of the u-velocity by the modified GAD as well as stronger azimuthal velocities.

Figure 4 also illustrates the differences between the original and modified GAD by looking at the time-average mean and variance of the u-velocity along a hub-height transverse profile at several up- and downstream distances from the turbine. The results are normalized by those of the simulation without turbines, whose results are also extracted at the same distances from the turbine and denoted with the subscript ∞.

Although, both the original and modified GAD results show transverse profiles with the same shape, i.e. double Gaussian in the near wake $(x-x_o)/D < 2$, and Gaussian further downstream $(x-x_o)/D > 4$, differences in the mean velocity are already noticed upstream of the rotor. At a distance of $(x-x_o)/D = -0.5$, the modified GAD portrays higher velocity deficits; the

https://doi.org/10.5194/egusphere-2026-6163
Preprint. Discussion started: 24 November 2026
© Author(s) 2026. CC BY 4.0 License.

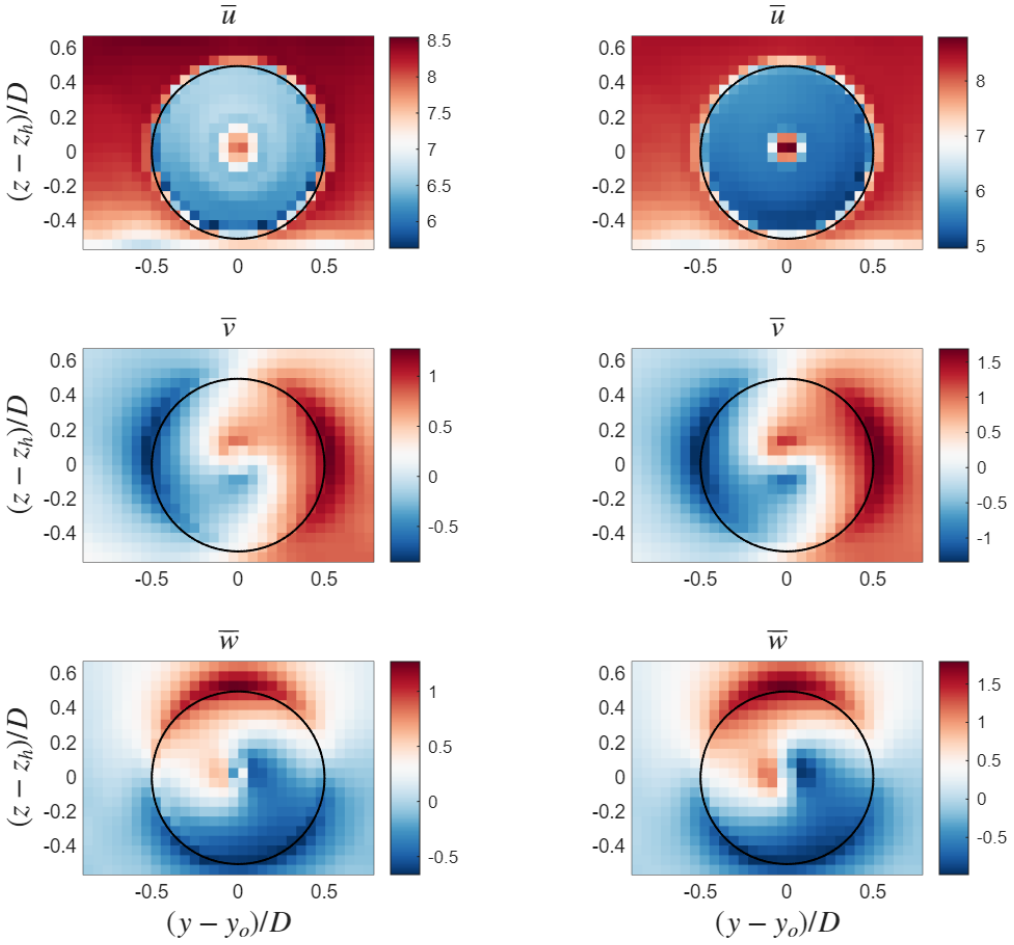

Figure 3. 30-min time-averaged vertical planes of the three velocity components (u-top, v-middle, w-bottom) at one grid point behind the turbine for the original BEM-based (left) and the modified GAD (right). The colorbar shows the velocity in m s^{-1} and the black circle the perimeter of the turbine rotor.

https://doi.org/10.5194/egusphere-2026-6163
Preprint. Discussion started: 24 November 2026
© Author(s) 2026. CC BY 4.0 License.

differences are enhanced within the near wake, and the results of both GADs become close to each other at $(x - x_o)/D = 8$. With regards to the u-variance, we do not notice changes upstream of the rotor as expected (Mann et al., 2018). Downstream of the rotor, both the original and modified GAD display similar shapes with u-variance values enhanced at the edge of the rotor as expected. However, at the transverse distances of enhanced variances, the modified GAD portrays higher values due to the larger local spatial gradients that the mean u-velocity profiles show.

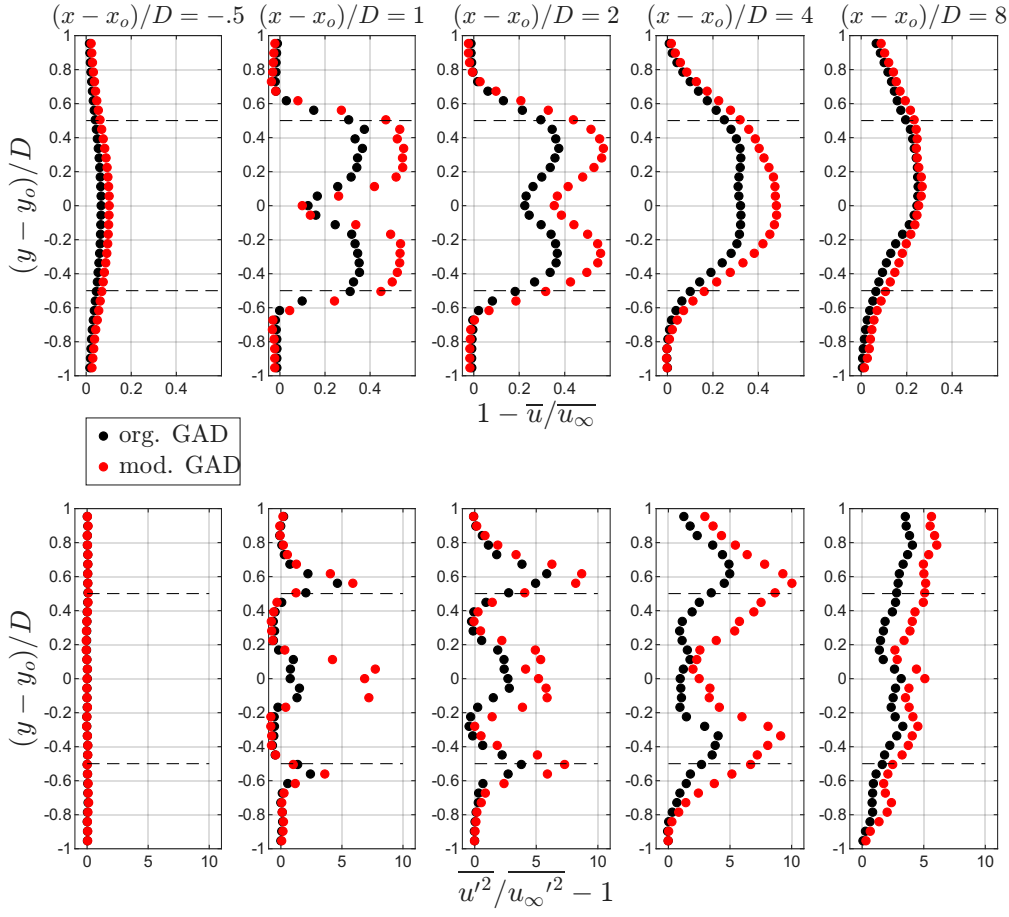

Figure 4. Hub-height transverse profiles of the 30-min mean (top) and variance (bottom) of the u-velocity component at five normalized up- and downstream distances $(x - x_o)/D$ for both the modified (mod.) GAD and the original (org.) GAD runs. The rotor extension is marked in dashed lines.

The velocity deficits from the modified GAD are higher than those from the original GAD mainly due to weaker azimuthal and normal forces computed by the original GAD procedure, as this uses the local velocities at the disk as a proxy of the free stream velocity. On the contrary and as explained in Sect. 4, the local (and generally lower) velocities are converted into free stream (and generally larger) velocities in the modified GAD procedure.

https://doi.org/10.5194/egusphere-2026-6163
Preprint. Discussion started: 24 November 2026
© Author(s) 2026. CC BY 4.0 License.

6.2 Wind farm cluster

For the cluster demonstration, we choose a real wind farm cluster layout, namely that of the N4 cluster in the German Bight without the Kaskasi wind farm, as shown in Fig. 5-left. In this figure, we rotate the N4 cluster 75°. The cluster consists of three wind farms: Amrumbank West with 80 Siemens SWT 3.6 MW wind turbines north of the cluster, Nordsee Ost with 48 Senvion SEN 6.15 MW wind turbines in the middle, and Meerwind with 80 Siemens SWT 3.6 MW wind turbines south of the cluster for a total of 208 wind turbines. The turbines in Nordsee Ost further use two types of blades (LM and RE); the thrust and performance curves are thus different for the same machine. This means that in practice there are three turbine types: for the full simulation, we create the files *wind-turbine-1.tbl*, *wind-turbine-2.tbl*, and *wind-turbine-3.tbl* for the Senvion LM, Senvion RE, and Siemens turbines, respectively. These files can be found in the repository with the modified GAD in Peña (2026), as well as the *windturb_spec* file called *globe_turbines.in* with the turbine layout and specifications.

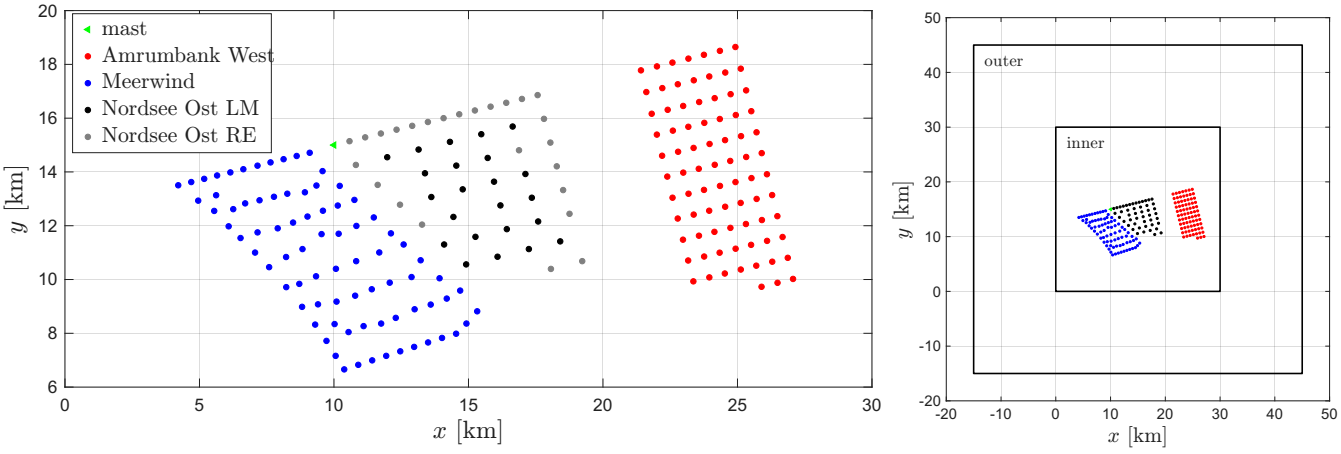

Figure 5. The layout of the N4 cluster used for the simulations. (left) The wind farms in the N4 cluster and the mast position. (right) The two-domains configuration of the idealized run with the outer and inner domains shown in black rectangles

6.2.1 Model setup

For this simulation, the configuration of the WRF model follows the description in Sect. 6.1.1 for the single wake verification, in terms of model physics and dynamics, and also uses a two-domains setup. Here, the u- and v-velocity components are initialized with values of 10.38 and -2.23 m s^{-1}, respectively. The outer domain is 60 km $\times$ 60 km with a horizontal grid spacing of 60 m. The inner domain is 30 km $\times$ 30 km with a horizontal spacing of 20 m: in this domain we include the turbines of the N4 cluster with the GAD. The two domains together with a description of the turbine cluster are shown in Fig. 5-right.

Both domains are run without turbines during eight hours, which we use as spin up time. The turbines are introduced after the spin up time in the inner domain and the domains are run for two hours more. Statistics of the LES fields are computed for the last hour of simulation. The full simulation with the three turbine types is performed with the modified GAD, but we also

https://doi.org/10.5194/egusphere-2026-6163
Preprint. Discussion started: 24 November 2026
© Author(s) 2026. CC BY 4.0 License.

perform a short 2-min simulation with the original BEM-based GAD to determine differences in the computational cost. Since the original GAD does not allow for three types of turbines, we use the DTU 10 MW turbine for all 208 turbine positions for the short simulation.

6.2.2 Results

For the cluster case, we output horizontal slices every 10 s of the three velocity components but, due to the size of the domain, only at the height that corresponds to the hub height of most turbines in the N4 cluster (87.5 m). Based on these slices, we perform statistics for the entire inner domain. Figure 6 shows the 1-hr mean and variance of the u-velocity component at 87.5 m within the inner domain. As illustrated in the mean field (Fig. 6-left), the velocity deficits from the wakes of Meerwind (the farm furthest to the left) easily reach the limits of the inner domain ≈20 km downstream of the farm: wakes that clearly impact both the closest wind farm (Nordsee Ost) and the furthest wind farm (Amrumbank West).

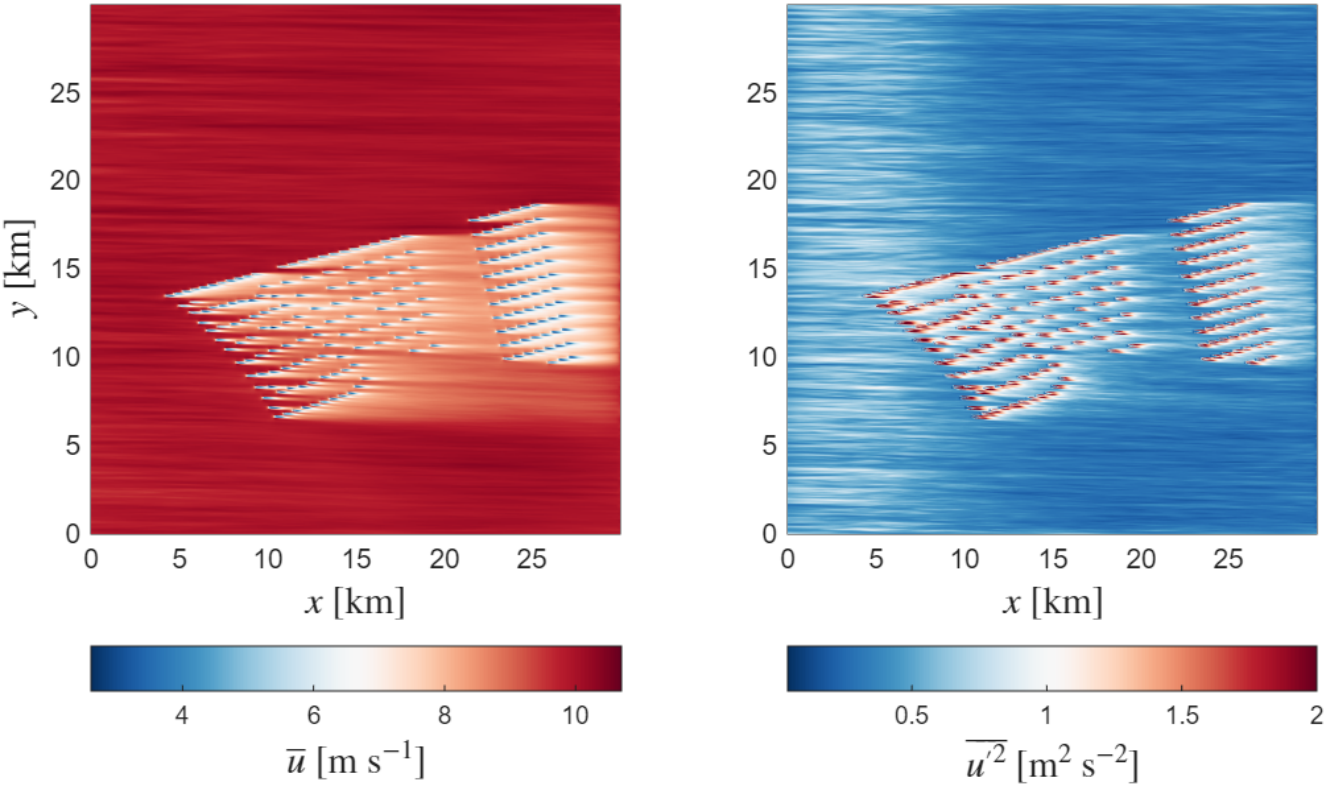

Figure 6. Horizontal plane of the 1-hr mean (left) and variance (right) of the u-velocity component at a height of 87.5 m within the inner domain using the modified GAD implementation.

As illustrated in the turbulent field (Fig. 6-right), in which we limit the upper values in the contour colorbar (maximum value of $\overline{u'^2}$ is 5.02 m s^{-2}) to better portray the regions with increased values behind the wind turbines, turbulence decays more

https://doi.org/10.5194/egusphere-2026-6163
Preprint. Discussion started: 24 November 2026
© Author(s) 2026. CC BY 4.0 License.

rapidly than the wake speed deficit. Thus, waked turbines within the same farm suffer from both reduced wind speeds and, for close turbine inter-spacings, increased turbulence levels. However, inter-farm turbulence effects do not appear that important for this cluster, flow direction, and atmospheric turbulence conditions. Notice that the minimum and maximum turbulence intensity $\sqrt{\overline{u'^2}}/\overline{u}$ values are 3.71% and 35% respectively. Also notice that although the domain extents for 30 km, for this two-domain setup, the first 5–10 km within inner domain clearly show the energetic transition from the bigger turbulence structures of the outer domain to the smaller turbulence scales of the inner domain.

Apart from the horizontal slices, we also output 1-s data of the simulated turbine performance that includes the parameters P, u_D, and yaw. In Fig. 7-left, which portrays an interpolated contour of the 1-hr mean of u_D, we highlight local features of the simulation. For this flow condition, the turbines in the upper edge of the three farms experience flow speed ups due to the cluster/farm geometries. Other local flow accelerations are evident at turbine 141 in the Meerwind wind farm and turbine 86 in Amrumbank West (highlighted in Fig. 7-left), although this latter farm is that experiencing generally the lowest local velocities of all three farms due to both intra- and inter-farm wake effects.

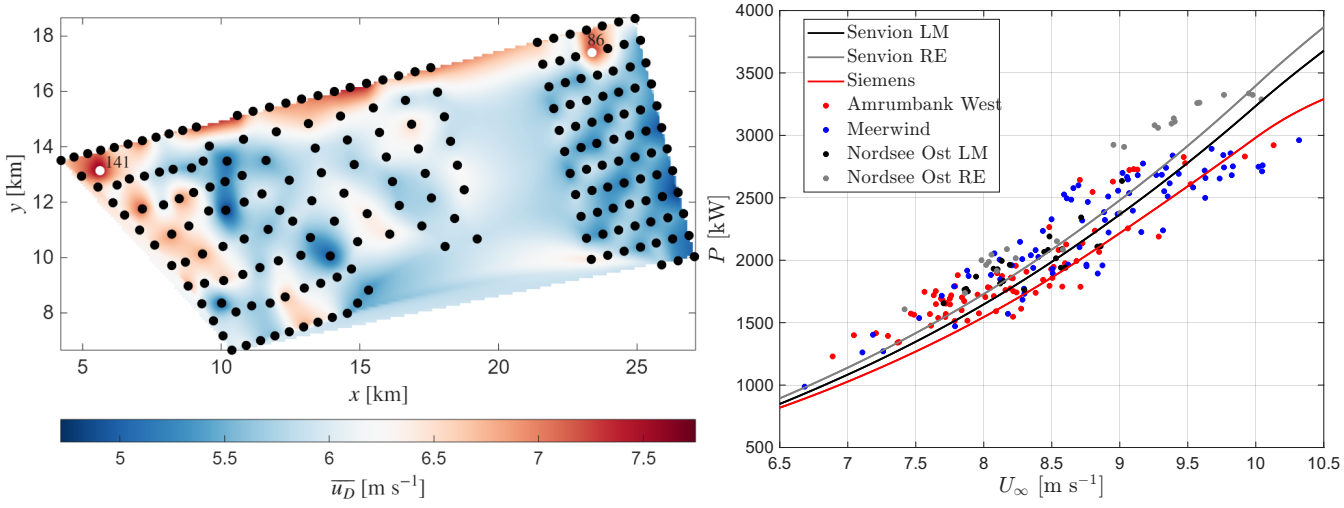

Figure 7. (left) Contour of the 1-hr disk-averaged velocity $\overline{u_D}$ at the position of the turbines (black circles) in the N4 cluster. Two turbines, 141 in Meerwind and 86 in Amrumbank West, are highlighted in white circles. (right) Power output as a function of the free-stream velocity for the turbines at the N4 cluster. The solid lines show the power curves of the different turbine types and the markers the 1-hr mean power output.

Figure 7-right illustrates the 1-hr mean power output of the 208 wind turbines in the N4 cluster, which are color-coded according to the farm they are associated to. The power curves of each of the turbine types are also displayed within a range of U_∞ values, which are computed by interpolating the tabulated data in the turbine files using the 1-hr $\overline{u_D}$ values. Amrumbank West and Meerwind show the largest ranges in U_∞ values due to the wakes. The power differences between the power curves and the simulated power are due to both wakes but also the complexity of the flow field around turbines that are not directly impacted by wakes.

https://doi.org/10.5194/egusphere-2026-6163
Preprint. Discussion started: 24 November 2026
© Author(s) 2026. CC BY 4.0 License.

7 Discussion and perspectives

In its present form, the computational cost of the modified GAD is similar to that of the original BEM-based GAD when used on a single wind turbine. For the single wind turbine case using the DTU 10 MW turbine, the original BEM-based GAD is 10% faster. However, for the cluster case, the modified GAD is 50% faster. This could be partly related to the BEM implementation as under the flow complexities of the cluster case, the iterative BEM procedure might become expensive. Note that the cluster case comparison is not fully fair as the BEM-based computations are performed with a bigger turbine as those used with the modified GAD. Also note that the modified GAD computations can be made faster by increasing the resolution (currently set to 1 m) at which we compute the radially-integrated coefficients in Sect. 2.

Although not shown in Fig. 4, we also compare the hub-height transverse profiles of the u-velocity component with analytical formulations of the velocity deficit commonly used in engineering wake models. Such an exercise is useful as these models remain the industry standard for wind farm design and optimization, albeit their inabilities, assumptions, and simplifications. In particular, we use the Gaussian-like models of Bastankhah and Porté-Agel (2014) and Pedersen et al. (2022) in which the velocity deficit has the form $1-u/u_\infty = C\exp\left(-(x-x_o)/(2\sigma^2)\right)$, where the maximum velocity deficit at the wake center is $C = 1-\sqrt{1-C_\mathrm{T}/\left(8(\sigma/D)^2\right)}$, with σ representing the wake width. The difference between these two wake velocity models is related to the formulation of the normalized wake expansion σ/D: in Bastankhah and Porté-Agel (2014), it linearly expands with downstream distance, whereas in Pedersen et al. (2022), the downstream expansion is non-linear (see details in their correspondent references). For the high C_T value of the single wake case (0.814), σ/D by Pedersen et al. (2022) becomes 7 to 22% higher within the range $1 \leq (x-x_o)/D \leq 4$, whereas it turns to be 10% lower at $(x-x_o)/D = 8$ compared to that by Bastankhah and Porté-Agel (2014). These differences result in a very good match of the maximum velocity deficit by the model by Pedersen et al. (2022) with the results of the modified GAD within $(x-x_o)/D \leq 4$; at $(x-x_o)/D \leq 4$ the model of Bastankhah and Porté-Agel (2014) causes no velocity deficit and at $(x-x_o)/D = 4$, it overestimates the maximum velocity deficit compared to the modified GAD results. However, at $(x-x_o)/D = 8$, the match of the maximum velocity deficit of the modified GAD is best with the model of Bastankhah and Porté-Agel (2014). Further, the model of Pedersen et al. (2022) also contains an expression of the wake-added turbulence, i.e. the normalized velocity variance $\overline{u'^2}/\overline{u'^2_\infty}-1$. Their expression, which originates from the work of Frandsen (2007), does not produce the downstream double-peak pattern shown in Fig. 4-bottom and tend to over- and underpredict the effect of the turbine on turbulence within the near and far wake, respectively. Future work should focus on comparison of wake-turbulence formulations with LESs aiming at studying inter- and intra-farm effects. As shown in our study, the modified GAD can serve as a reference tool for such work.

The modified GAD is currently being used for real-time multiscale atmospheric simulations of wind turbine clusters, where the WRF outermost domain is forced with a reanalysis product and turbines are introduced in the innermost LES domain. Although computationally expensive, the most difficult challenge we nowadays face, when performing such multiscale simulations, is related to validation as there are only a couple of wind farm clusters where turbine SCADA time series are available.

https://doi.org/10.5194/egusphere-2026-6163
Preprint. Discussion started: 24 November 2026
© Author(s) 2026. CC BY 4.0 License.

8 Conclusions

A consistent and generalized actuator disk was implemented into the WRF model for LES based on the generalized body forces by Sørensen (2023) and the existing AD procedure implemented into the WRF model by Mirocha et al. (2014). This modified implementation was verified against the original BEM-based GAD developed for WRF-LES by Mirocha et al. (2014) for a single wind turbine on a neutral atmospheric boundary layer. The shape and patterns of the velocity deficits and variances between both GADs resemble each other. However, the velocity deficits from the modified GAD are higher than those from the original GAD mainly due to weaker azimuthal and normal forces computed by the original GAD procedure as this uses the local velocities at the disk as a proxy of the free stream velocity. The stronger gradients in the velocity field lead to larger velocity variances in the wake of the turbine for the modified GAD runs. The modified GAD was also used to affordably simulate the N4 wind farm cluster in the German Bight, which consists of 208 turbines within three wind farms of three turbine types. The cluster results show the challenges that exist both in terms of mean velocities and turbulence within and between wind farms and the need for high-resolution simulations to accurately simulate the flow field and the performance of turbines.

Code and data availability. The model development is archived at https://doi.org/10.11583/DTU.33425044 (García-Santiago, 2026), which provides the source files required to integrate the implementation into a user's WRF source tree. The archive also includes a compressed copy of the exact WRF version used in this study (v4.2.1), together with the minimum set of files required to run the original GAD formulation and the airfoil data associated with the DTU 10 MW RWT. The input files required to run the single wake and the cluster cases, as well as readme files for the modified and original GAD versions implemented in the WRF model are archived at https://doi.org/10.11583/DTU.33060437 (Peña, 2026).

Author contributions. AP implemented the generalized turbine forces framework and modified the original procedure to account for these forces within the WRF model, performed the simulations and the analyses, and wrote the initial draft. OGS quality-controlled the modified GAD, MPvdL provided guidance for the modified procedure to account for the GAD forces and tabulated data for the wind turbine specific files, and BK and JM developed and provided assistance with the original GAD. All authors revised and edited the manuscript.

Competing interests. The authors declare that they have no competing interests.

Acknowledgements. The work is partly funded by the DTEC cooperation between DTU Wind and Energy Systems and TotalEnergies, and by CETPartnership, the Clean Energy Transition Partnership under the 2023 joint call for research proposals, co-funded by the European Comission (GA 101 069750) and with the funding organiations detailed on https://cetpartnership.eu/funding-agencies-and-call-modules. Work by JM was performed under the auspices of the U.S. Department of Energy by Lawrence Livermore National Laboratory under

https://doi.org/10.5194/egusphere-2026-6163
Preprint. Discussion started: 24 November 2026
© Author(s) 2026. CC BY 4.0 License.



Contract DE-AC52-07NA27344. We also acknowledge the computational and data resources provided on the Sophia HPC Cluster at the Technical University of Denmark, DOI: 10.57940/FAFC-6M81.

https://doi.org/10.5194/egusphere-2026-6163
Preprint. Discussion started: 24 November 2026
© Author(s) 2026. CC BY 4.0 License.

References

Ainslie, J. F.: Calculating the flowfield in the wake of wind turbines, J. Wind Eng. Ind. Aerodyn., 27, 213–224, 1988.

Archer, C. L., Wu, S., Ma, Y., and Jimenez, P. A.: Two corrections for turbulent kinetic energy generated by wind farms in the WRF model, Mon. Wea. Rev., 148, 4823–4835, https://doi.org/10.1175/MWR-D-20-0097.1, 2020.

Arthur, R. S., Mirocha, J. D., Marjanovic, N., Hirth, B. D., Schroeder, J. L., Wharthon, S., and Chow, F. K.: Multi-scale simulation of wind farm performance during a frontal passage, Atmosphere, 11, 245, https://doi.org/https://doi.org/10.3390/atmos11030245, 2020.

Bak, C., Zahle, F., Bitsche, R., Kim, T., Yde, A., Henriksen, L. C., Natarajan, A., and Hansen, M. H.: Description of the DTU 10 MW reference turbine, Tech. Rep. DTU Wind Energy Report-I-0092, Technical University of Denmark, 2013.

Bastankhah, M. and Porté-Agel, F.: A new analytical model for wind-turbine wakes, Renew. Energ., 70, 116–123, https://doi.org/10.1016/j.renene.2014.01.002, 2014.

Betz, A.: Schraubenpropeller mit geringstem Energieverlust. Mit einem Zusatz von l. Prandtl, Nachrichten von der Gesellschaft der Wissenschaften zu Göttingen, Mathematisch-Physikalische Klasse, 1919, 193–217, 1919.

Bleeg, J., Purcell, M., Ruisi, R., and Traiger, E.: Wind farm blockage and the consequences of neglecting its impact on energy production, Energies, 11, https://doi.org/https://doi.org/10.3390/en11061609, 2018.

Brown, K., Bortolotti, P., Branlard, E., Chetan, M., Dana, S., deVelder, N., Doubrawa, P., Hamilton, N., Ivanov, H., Jonkman, J., Kelley, C., and Zalkind, D.: One-to-one aeroservoelastic validation of operational loads and performance of a 2.8 MW wind turbine model in OpenFAST, Wind Energ. Sci., 9, 1791–1810, https://doi.org/10.5194/wes-9-1791-2024, 2024.

Bui, H., Bakhoday-Paskyabi, M., and Mohammadpour-Penchah, M.: Implementation of a simple actuator disk for large-eddy simulation in the Weather Research and Forecasting model (WRF-SADLES v1.2) for wind turbine wake simulation, Geosci. Model Dev., 17, 4447–4465, https://doi.org/10.5194/gmd-17-4447-2024, 2024.

Deardorff, J. W.: Stratocumulus-capped mixed layers derived from a three-dimensional model, Boundary-Layer Meteorol., 18, 495–527, 1980.

Dörenkämper, M., Vollmer, L., and Lakdawala, Z.: Simulating the impact of offshore wind expansion on yield and efficiency in the North Sea by 2050, Research report, Fraunhofer Institute for Wind Energy Systems (IWES), Oldenburg, Germany, 2025.

DTU Wind and Energy Systems: PyWakeEllipSys v5.4, https://topfarm.pages.windenergy.dtu.dk/cuttingedge/pywake/pywake_ellipsys/, 2025.

Du, B., Ge, M., Li, X., and Liu, Y.: A meso-microscale coupled wind farm parameterization, Boundary-Layer Meteorol., 191, 35, https://doi.org/https://doi.org/10.1007/s10546-025-00928-7, 2025.

Fischereit, J., Vedel, H., Larsén, X. G., Theeuwes, N. E., Giebel, G., and Kaas, E.: Modelling wind farm effects in HARMONIE–AROME (Cycle 43.2.2) – Part 1: Implementation and evaluation, Geosci. Model Dev., 17, 2855–2875, https://doi.org/10.5194/gmd-17-2855-2024, 2024.

Fitch, A. C., Olson, J. B., Lundquist, J. K., Dudhia, J., Gupta, A. K., Michalakes, J., and Barstad, I.: Local and mesoscale impacts of wind farms as parameterized in a mesoscale NWP model, Mon. Wea. Rev., 140, 3017–3038, https://doi.org/10.1175/MWR-D-11-00352.1, 2012.

Frandsen, S. T.: Turbulence and turbulence-generated structural loading in wind turbine clusters, Tech. Rep. Risoe-R-1188(EN), Risø DTU, 2007.

https://doi.org/10.5194/egusphere-2026-6163
Preprint. Discussion started: 24 November 2026
© Author(s) 2026. CC BY 4.0 License.

Gaertner, E., Rinker, J., Sethuraman, L., Zahle, F., Anderson, B., Barter, G., Abbas, N., Meng, F., Bortolotti, P., Skrzypinski, W., Scott, G., Feil, R., Bredmose, H., Dykes, K., Shields, M., Allen, C., , and Viselli, A.: Definition of the IEA 15-Megawatt Offshore Reference Wind, Tech. Rep. NREL/TP-5000-75698, National Renewable Energy Laboratory, 2020.

García-Santiago, O.: Source code for 'A consistent and generalized actuator disk for the WRF model', Technical University of Denmark. Dataset. DOI:10.11583/DTU.33425044, 2026.

García-Santiago, O., Hahmann, A. N., Badger, J., and Peña, A.: Evaluation of wind farm parameterizations in the WRF model under different atmospheric stability conditions with high-resolution wake simulations, Wind Energ. Sci., 9, 963–979, https://doi.org/https://doi.org/10.5194/wes-9-963-2024, 2024.

Hahmann, A. N., Imberger, M., Fischereit, J., de Linaje, N. G. A., and Badger, J.: Environmental mapping and screening of the offshore wind potential in Denmark: sensitivity mapping: wind, Tech. rep., DTU Wind and Energy Systems, Roskilde, Denmark, 2025.

Jensen, N. O.: A note on wind generator interaction, Tech. Rep. Risoe-M-2411(EN), Risø National Laboratory, 1983.

Jonkman, J., Butterfield, S., Musial, W., and Scott, G.: Definition of a 5-MW reference wind turbine for offshore system development, Tech. Rep. NREL/TP-500-38060, National Renewable Energy Laboratory, 2012.

Kale, B., Buckingham, S., van Beeck, J., and Cuerva-Tejero, A.: Implementation of a generalized actuator disk model into WRF v4.3: A validation study for a real-scale wind turbine, Renew. Energy, 197, 810–827, https://doi.org/10.1016/j.renene.2022.07.119, 2022.

Lissaman, P. B. S.: Energy effectiveness of arbitrary arrays of wind turbines, J. Energy, 3, 323–328, 1979.

Ma, Y., Archer, C. L., and Vasel-Be-Hagh, A.: The Jensen wind farm parameterization, Wind Energ. Sci., 7, 2407–2431, https://doi.org/10.5194/wes-7-2407-2022, 2022a.

Ma, Y., Archer, C. L., and Vasel-Be-Hagh, A.: Comparison of individual versus ensemble wind farm parameterizations inclusive of sub-grid Wakes for the WRF model, Wind Energ., 25, 1573–1595, https://doi.org/10.1002/we.2758, 2022b.

Mann, J., Peña, A., Troldborg, N., and Andersen, S. J.: How does turbulence change approaching the rotor?, Wind Energ. Sci., 3, 293–300, https://doi.org/10.5194/wes-3-293-2018, 2018.

Marjanovic, N., Mirocha, J. D., Kosović, B., Lundquist, J. K., and Chow, F. K.: Implementation of a generalized actuator line model for wind turbine parameterization in the Weather Research and Forecasting model, J. Renew. Sustain. Energ., 9, 063 308, https://doi.org/10.1063/1.4989443, 2017.

Mikkelsen, R.: Actuator disc methods applied to wind turbines, Tech. Rep. MEK-FM-PHD 2003-02, Technical University of Denmark, 2003.

Mirocha, J. D., Kosović, B., Aitken, M. L., and Lundquist, J. K.: Implementation of a generalized actuator disk wind turbine model into the Weather Research and Forecasting model for large-eddy simulation applications, J. Renew. Sustain. Energ., 6, 013 104, https://doi.org/10.1063/1.4861061, 2014.

Pedersen, J. G., Svensson, E., Poulsen, L., and Nygaard, N. G.: Turbulence optimized Park model with Gaussian wake profile, J. Phys.: Conf. Series, 2265, 022 063, https://doi.org/10.1088/1742-6596/2265/2/022063, 2022.

Peña, A., Mirocha, J. D., and van der Laan, M. P.: Evaluation of the Fitch wind-farm wake parametrization with large-eddy simulations of wakes using the Weather Research and Forecasing model, Mon. Wea. Rev., 150, 3051–3064, https://doi.org/10.1175/MWR-D-22-0118.1, 2022.

Peña, A.: Dataset and input files for "A consistent and generalized actuator disk for the WRF model", Technical University of Denmark. Dataset. DOI:10.11583/DTU.33060437, 2026.

Peña, A. and Angelou, N.: The wake wrecker: a special case of a shallow low-level jet simulation impacting a turbine in WRF-LES, J. Phys.: Conf. Ser., 3016, 012 043, https://doi.org/10.1088/1742-6596/3016/1/012043, 2025.

https://doi.org/10.5194/egusphere-2026-6163
Preprint. Discussion started: 24 November 2026
© Author(s) 2026. CC BY 4.0 License.



Sanchez Gomez, M., Lundquist, J. K., Mirocha, J. D., and Arthur, R. S.: Investigating the physical mechanisms that modify wind plant blockage in stable boundary layers, Wind Energ. Sci., 8, 1049–1069, https://doi.org/10.5194/wes-8-1049-2023, 2023.

Sanchez-Gomez, M., Deskos, G., Optis, M., Lundquist, J. K., Sinner, M., Xia, G., and Musial, W.: Differences in cluster and internal wake effects from mesoscale and large-eddy simulations off the US East Coast, Wind Energ. Sci., 11, 2009–2036, https://doi.org/10.5194/wes-11-2009-2026, 2026.

Sørensen, J. N.: Generalized analytical body force model for actuator disc computations of wind turbines, Wind Energ. Sci., 8, 1017–1027, https://doi.org/10.5194/wes-8-1017-2023, 2023.

Sørensen, N. N.: General purpose flow solver applied to flow over hills, Ph.D. thesis, Risø National Laboratory, Roskilde, Denmark, 1994.

Sørensen, J. N., Nilsson, K., Ivanell, S., Asmuth, H., and Mikkelsen, R. F.: Analytical body forces in numerical actuator disc model of wind turbines, Renew. Energy, 147, 2259–2271, https://doi.org/10.1016/j.renene.2019.09.134, 2020.

The MathWorks Inc.: MATLAB version 9.16 (R2024a), https://www.mathworks.com, 2024.

Troldborg, N.: Actuator line modeling of wind turbine wakes, Tech. rep., PhD Thesis, Technical University of Denmark, 2008.

van der Laan, M., Andersen, S., Kelly, M., and Baungaard, M.: Fluid scaling laws of idealized wind farm simulations, J. Phys.: Conf. Ser., 1618, 062 018, https://doi.org/10.1088/1742-6596/1618/6/062018, 2020.

van der Laan, M. P., Sørensen, N. N., Réthoré, P.-E., Mann, J., Kelly, M. C., and Troldborg, N.: The k-ε-f_P model applied to double wind turbine wakes using different actuator disk force methods, Wind Energ., 18, 2223–2240, https://doi.org/https://doi.org/10.1002/we.1816, 2015.

van Stratum, B., Theeuwes, N., Barkmeijer, J., van Ulft, B., and Wijnant, I.: A one-year-long evaluation of a wind-farm parameterization in HARMONIE-AROME, J. Adv. Model. Earth Syst., 14, e2021MS002 947, https://doi.org/10.1029/2021MS002947, 2022.

Vermeer, L. J., Sørensen, J. N., and Crespo, A.: Wind turbine wake aerodynamics, Progr. Aerospace Sci., 39, 467–510, 2003.

Volker, P. J. H., Badger, J., Hahmann, A. N., and Ott, S.: The Explicit Wake Parametrisation V1.0: a wind farm parametrisation in the mesoscale model WRF, Geosci. Model Dev., 8, 3715–3731, https://doi.org/10.5194/gmd-8-3715-2015, 2015.

Wu, S., Archer, C. L., and Mirocha, J. D.: New insights on wind turbine wakes from large-eddy simulation: Wake contraction, dual nature, and temperature effects, Wind Energ., 27, 1130–1151, https://doi.org/https://doi.org/10.1002/we.2827, 2024.

Zahle, F., Barlas, A., Lønbæk, K., Bortolotti, P., Zalkind, D., Wang, L., Labuschagne, C., Sethuraman, L., and Barter, G.: Definition of the IEA wind 22-Megawatt offshore reference wind turbine, Tech. Rep. DTU Wind Energy Report E-0243, DTU Wind and Energy Systems, 2024.